

## VIP Aluminium Compounds Very Important Paper

How to cite: *Angew. Chem. Int. Ed.* **2021**, *60*, 24702–24708

International Edition: doi.org/10.1002/anie.202111385

German Edition: doi.org/10.1002/ange.202111385

## Reversible Dissociation of a Dialumene\*\*

Rosalyn L. Falconer, Keelan M. Byrne, Gary S. Nichol, Tobias Krämer,\* and Michael J. Cowley\*

**Abstract:** Dialumenes are neutral Al<sup>I</sup> compounds with Al=Al multiple bonds. We report the isolation of an amidophosphine-supported dialumene. Our X-ray crystallographic, spectroscopic, and computational DFT analyses reveal a long and extreme trans-bent Al=Al bond with a low dissociation energy and bond order. In solution, the dialumene can dissociate into monomeric Al<sup>I</sup> species. Reactivity studies reveal two modes of reaction: as dialumene or as aluminyl monomers.

## Introduction

Like other low oxidation-state main group systems, Al<sup>I</sup> compounds are revealing potential in bond-activation and catalysis.<sup>[1]</sup> Dialumenes are neutral Al<sup>I</sup> compounds with Al=Al multiple bonds. They sit alongside the prototypical neutral Al<sup>I</sup> compounds (Cp\*Al)<sub>4</sub> and NaCNacAl(I), and the rapidly developing class of anionic aluminyl compounds.<sup>[2]</sup>

Dialumenes can be divided into two classes: base-coordinated dialumenes (R(L)Al=Al(L)R), which are iso-electronic with alkenes, and “transient” dialumenes (RAI=AIR). Two base-coordinated dialumenes have been reported. The first, silyl substituted **I**, was reported by Inoue in 2017.<sup>[3a]</sup> An aryl analogue, **II**, followed (Figure 1).<sup>[3b]</sup> Though base-free dialumenes (**III**) are yet to be isolated, “masked” examples that behave as RAI=AIR are known. Power reported the toluene adduct **IV**,<sup>[4]</sup> and Tokitoh the related benzene adduct **V**.<sup>[5]</sup>

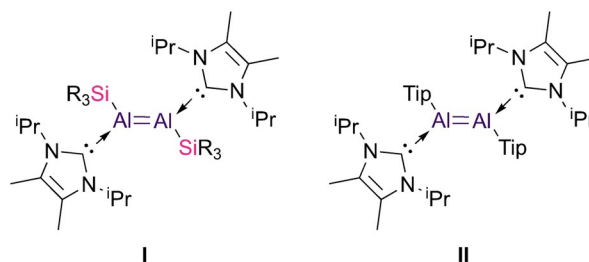
Dialumenes readily activate dihydrogen and other small molecules.<sup>[5,6]</sup> Inoue’s **I** and **II** catalytically reduce CO<sub>2</sub> with HBPIn.<sup>[3b,7]</sup> This capability comes from closely-spaced frontier molecular orbitals, which beget high reactivity. Even considering the only isolated examples, **I** and **II**, it is clear that understanding the interplay between substituents, bonding,

and reactivity in dialumenes is critical to their further development.

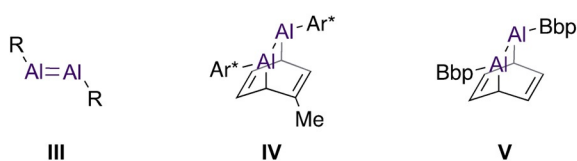
Base-coordinated and base-free dialumenes are clearly related, but insights from experiment and theory reveal very different pictures of bonding. Dialumenes **I** and **II** feature planar or moderately trans-bent Al=Al bonds with double bond character, do not dissociate, and react as dialumenes. In contrast, donor-free dialumenes **III** feature low Al=Al bond orders and substantially trans-bent geometry.<sup>[8]</sup> These dialumenes can dissociate readily in solution; **V** appears to react as either RAI=AIR or RAl: species.<sup>[9]</sup> Recently, Power showed that a larger terphenyl substituent allows access to an RAl: monomer rather than **IV**.<sup>[10]</sup>

A transient N,P-coordinated aluminyl monomer was implicated in our recent studies of reductive elimination in the Al(II) dihydrodialane **VI** (Figure 1 c).<sup>[11]</sup> We thus targeted isolable Al<sup>I</sup> compounds of the same amidophosphine ligand.

## a) Base-coordinated dialumenes



## b) Transient and ‘masked’ dialumenes



## c) Reversible reductive elimination in an Al(II) dihydride

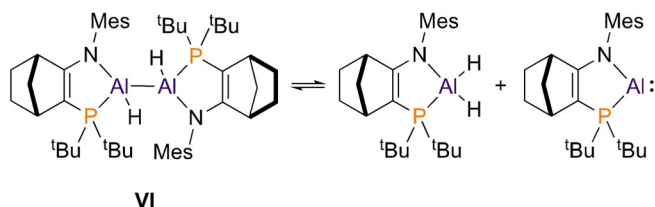


**Figure 1.** a) Base-coordinated dialumenes (R<sub>3</sub>Si = Me<sup>t</sup>Bu<sub>2</sub>Si; Tip = 2,4,6-triisopropylphenyl). b) “masked” dialumenes (Ar\* = 2,6-(2,6-diisopropylphenyl)phenyl; Bbp = 2,6-(bis(trimethylsilyl)methyl)phenyl). c) Reversible reductive elimination in **VI** (Mes = 2,4,6-trimethylphenyl).

[\*] Dr. R. L. Falconer, Dr. G. S. Nichol, Dr. M. J. Cowley  
School of Chemistry, University of Edinburgh  
Edinburgh (UK)  
E-mail: michael.cowley@ed.ac.uk

K. M. Byrne, Dr. T. Krämer  
Department of Chemistry, Maynooth University  
Maynooth, Co. Kildare (Ireland)  
E-mail: tobias.kraemer@mu.ie

[\*\*] A previous version of this manuscript has been deposited on a preprint server (<https://doi.org/10.33774/chemrxiv-2021-6443s>).

Supporting information and the ORCID identification number(s) for the author(s) of this article can be found under:  
<https://doi.org/10.1002/anie.202111385>.

© 2021 The Authors. Angewandte Chemie International Edition published by Wiley-VCH GmbH. This is an open access article under the terms of the Creative Commons Attribution License, which permits use, distribution and reproduction in any medium, provided the original work is properly cited.

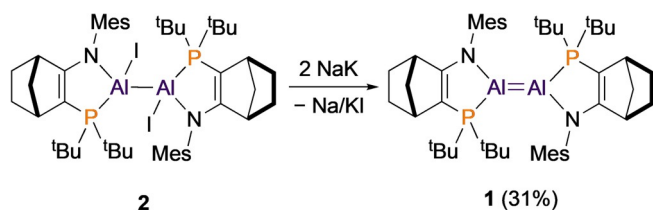
We report here the base-coordinated dialumene **1**. Our studies demonstrate that **1** has an unusually weak Al=Al bond with low bond-order and an extreme trans-bent geometry. We reveal how the amidophosphine ligand of **1** is the origin of these effects. In solution, **1** dissociates and can react as either dialumene or monomeric aluminyl.

## Results and Discussion

We prepared dialumene **1** by reduction from the Al(II) precursor diiododialane **2** (Scheme 1). Treatment of **2** with 2 equiv Na/K alloy in THF led to a colour change from yellow to dark purple. After 5 hours,  $^{31}\text{P}\{^1\text{H}\}$  NMR spectroscopy revealed consumption of **2** and a new broad resonance at  $\delta$  21.3, as well as minor amounts of dihydrodialane **VI**. Crystalline dialumene **1** was isolated as a dark purple solid in 31% yield from toluene at  $-30^\circ\text{C}$ . UV/vis spectroscopy revealed  $\lambda_{\text{max}}$  567.0 nm, which we assign to a  $\pi$  to  $\pi^*$  transition (Figure S3, Table S10). At 293 K, **1** decomposes over 1–2 days in THF, toluene or hexane solutions.

The solid-state structure of dialumene **1**, determined by X-ray crystallography, reveals a highly trans-bent Al=Al bond in *E* configuration (Figure 2). Two-site disorder of the Al positions reveals major and minor isomers of **1** (88/12%) with distinct geometries around the Al<sub>2</sub> core. The amidophosphine ligands enforce narrow N1–Al1–P1 angles (83–84°). The Al=Al distance in **1** is shorter by 0.1–0.2 Å than in the related Al(II) dihydrodialane **VI** or in Uhl's dialane(4) ((SiMe<sub>3</sub>)<sub>2</sub>HC)<sub>2</sub>Al–Al(CH(SiMe<sub>3</sub>)<sub>2</sub>)<sub>2</sub> (**I** 2.5190(14)/2.471(13) Å; **VI** 2.6586(16) Å; Uhl's dialane 2.660(1) Å).<sup>[12]</sup> Nevertheless, the Al=Al distance in **1** is notably longer (~0.1 Å) than in Inoue's dialumenes [**I** 2.3943(16); **II** 2.4039(8)]. Compared to **I** and **II**, the Al=Al core of **1** is much less planar (**1**  $\theta = 48.8^\circ/51.2^\circ$ ; **I**:  $0^\circ$ ; **II**:  $17.3^\circ/23.7^\circ$ ). We note that the pyramidalised Al centres in **1** are stereogenic; the major and minor isomers in the solid-state structure have opposite stereochemistry at the Al centres.

DFT calculations reveal that the bonding situation in **1** is distinct from previous base-coordinated dialumenes **I** and **II**. Natural Bond Orbital (NBO) analysis of **1** shows natural localised molecular orbitals (NLMOs) representing Al–Al  $\sigma$ - and  $\pi$ -bonds (Figure 3 a). Although it retains some apparent  $\pi$ -bond character, the corresponding NLMO of **1** is heavily localised on the aluminium centres; the relevant NLMOs of **I** or **II** more closely resemble classical  $\pi$ -orbitals (Figure S19/20). The localisation of the  $\pi$ -orbital in dialumene **1** results from admixture of the Al–Al  $\sigma^*$ . The extent of this admixture is revealed by the increased s-character of the NLMO of



Scheme 1. Preparation of dialumene **1**.

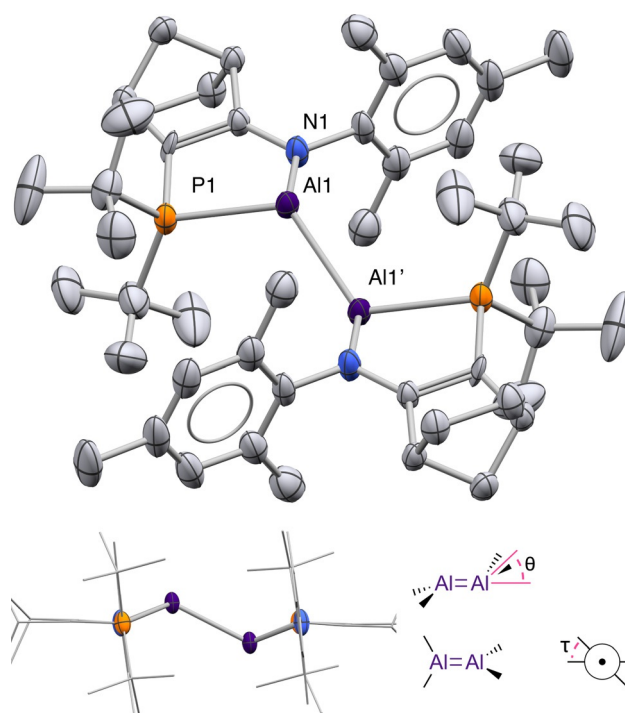
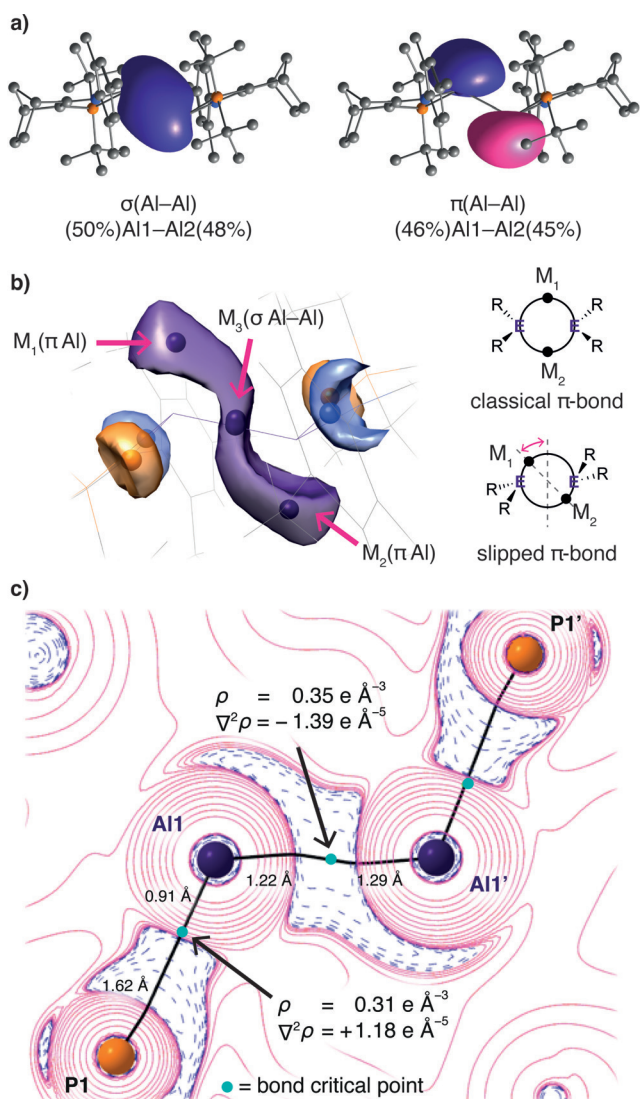


Figure 2. X-ray crystal structure of dialumene **1** (H atoms omitted for clarity). Thermal ellipsoids at 50% probability. Major component of disordered Al/ligand displayed (**1A**). Selected bond distances [Å] and angles [°]: Al1–Al1' 2.5190(14); N1–Al1 1.909(2); P1–Al1 2.4816(9); N1–Al1'–P1 84.86(7);  $\theta = 48.8$ ;  $\tau = 0.21$ .

**1** (Al1/Al2  $\text{sp}^{1.25}/\text{sp}^{1.09}$ ) compared to that in, for example, **II** (Al1/Al2  $\text{sp}^{48.34}/\text{sp}^{23.32}$ ), where the  $\pi$ -bond is constructed from essentially pure p-orbitals. Consistent with this picture, the Wiberg bond index for the Al=Al bond of **1** is 1.31, which is increased from that of dihydrodialane **VI** (0.91) but lower than in **I** or **II** (1.67, 1.54).

Grützmacher and Fässler have proposed simple topographical criteria for distinguishing classical and non-classical multiple bonds.<sup>[13]</sup> Their criteria use the Electron Localisation Function (ELF), which identifies regions of localised valence electron density. The ELF of classically  $\pi$ -bonded systems reveals “attractors”—local maxima *M* in the ELF that correspond to electron pairs—above and below the plane of E=E bonds. Each attractor *M* is surrounded by a “basin” of electron density. The topology and electron population of such basins is interpretable in familiar terms as covalent bonds or lone pairs. Classical  $\pi$ -bonded systems have “dumb-bell” shaped electron basins, and their populations sum to approximately  $4e^-$ .

Topological analysis of the ELF of **1** (Figure 3 b) reveals a quite different picture. The characteristic pattern of attractors and basins for a slipped  $\pi$ -bond is observed. Three valence attractors, *M*<sub>1</sub>–*M*<sub>3</sub>, are found near the Al<sub>2</sub> unit. *M*<sub>3</sub> is centred on the Al–Al bond; its basin population is  $1.11e^-$ . *M*<sub>1</sub> and *M*<sub>2</sub> are each above or below an Al centre, “slipped” from their positions in a classical double bond. The basins of *M*<sub>1</sub>/*M*<sub>2</sub> are each populated by  $\sim 1.30e^-$ ; the summed basin populations ( $3.76e^-$ ) correspond with the  $4e^-$  available for bonding from the two Al<sup>I</sup> centres of **1**.



**Figure 3.** Electronic structure analysis of **1**. a) NLMOs (isovalue = 0.036) of the Al=Al bond. b) ELF localisation domains (isovalue = 0.795) of the Al=Al core.  $M_n$  indicates attractors. c) Laplacian of the electron density in the P–Al=Al–P plane. Areas of charge concentration and depletion (blue/pink), bond paths (black) and bond critical points shown.

The positions of attractors  $M_1$ – $M_3$  in **1** correspond with those in the base-free dialumene  $\text{Al}_2\text{H}_2$ .<sup>[8a,14]</sup> The sigmoidal form of the ELF isosurface of **1** is a feature of bonding in base-free dialumenes, along with low Al–Al bond order ( $\sim 0.5$ ) and diradical character.<sup>[8a]</sup> Based on the basin population around  $M_3$  ( $1.11 e^-$ ), **1** also has low Al–Al bond order.  $M_1$  and  $M_2$  can be interpreted as non-bonding electron density at Al. In contrast, the ELF of planar dialumene **I** reveals features of classical  $\pi$ -bonds: an attractor on each face of the Al=Al bond (Figure S23).

To better determine the Al–Al bond order in **1**, we undertook Quantum Theory of Atoms in Molecules (QTAIM) analysis (Figure 3c and SI). The molecular graph reveals Al–Al, Al–N and Al–P bond paths. The Al–P interactions are polar dative bonds, as revealed by the position of their bond critical points (bcp) closer to the more

electropositive Al centres and associated QTAIM parameters ( $\sigma_{\text{bcp}} = 0.310 \text{ e \AA}^{-3}$ ,  $\nabla^2\sigma_{\text{bcp}} = +1.180 \text{ e \AA}^{-5}$ ,  $H_{\text{bcp}} = -0.107 E_h \text{ \AA}^{-3}$ ,  $G_{\text{bcp}}/\sigma_{\text{bcp}} < 1$ ).<sup>[15]</sup> Meanwhile the Al–N bonds exhibit stronger ionic character ( $\sigma_{\text{bcp}} = 0.499 \text{ e \AA}^{-3}$ ,  $\nabla^2\sigma_{\text{bcp}} = +8.410 \text{ e \AA}^{-5}$ ,  $H_{\text{bcp}} = -0.094 E_h \text{ \AA}^{-3}$ ,  $G_{\text{bcp}}/\sigma_{\text{bcp}} < 1$ ). The Al–Al bond features weak shared-shell covalent character, as judged by the charge concentration and topological parameters at its bcp ( $\sigma_{\text{bcp}} = 0.349 \text{ e \AA}^{-3}$ ,  $\nabla^2\sigma_{\text{bcp}} = -1.390 \text{ e \AA}^{-5}$ ,  $H_{\text{bcp}} = -0.135 E_h \text{ \AA}^{-3}$ ,  $G_{\text{bcp}}/\sigma_{\text{bcp}} < 1$ ). In accordance with the ELF results, the values of both  $\sigma_{\text{bcp}}$  and  $\nabla^2\sigma_{\text{bcp}}$  are rather low, indicating a weak Al–Al bond. The bond ellipticity parameter suggests a small degree of double bond character ( $\epsilon_{\text{bcp}} = 0.195$ ).

The delocalisation index  $\delta(\text{A},\text{B})$  is a quantitative measure for the number of electron pairs exchanged between two atomic basins. When referenced against a chemically-similar comparator compound with a well-defined bonding situation, the delocalisation index can reflect chemical bond order. Here, we use  $\delta(\text{Al},\text{Al})$  of the bond in dihydrodialane **VI** to define an Al–Al bond order of 1. At 0.65,  $\delta(\text{Al},\text{Al})$  in **VI** is about half that in the planar transition state **TS<sub>1C-1C</sub>** (see later) which unequivocally has a planar Al=Al double bond ( $\delta(\text{Al},\text{Al}) = 1.21$ ). In trans-bent dialumene **1**,  $\delta(\text{Al},\text{Al})$  at 0.80 is only slightly higher than that of dihydrodialane **VI**, but much lower than that of the Al=Al double-bond.<sup>[14]</sup>

The combined results of our crystallographic and electronic structure analyses indicate small but significant Al=Al multiple bond character in **1**. Al–Al bond distance, and computational bond order and delocalisation-index criteria all support the conclusion that the Al=Al bond in **1** is intermediate between single and double bonds, with bond order  $\sim 1.3$ .

Why is dialumene **1** so different from **I** and **II**? We used DFT calculations on a set of minimal base-coordinated dialumenes with NHC or  $\text{PMe}_3$  donors and hydride, phenyl, silyl or amino substituents (Table 1) to answer this question.<sup>[16]</sup>

The structures of the model dialumenes depend strongly on the substituent and Lewis base (NHC or  $\text{PMe}_3$ ). Electropositive substituents ( $\text{SiMe}_3$ ) provoke shorter Al=Al bonds, wider R–Al–L angles, and more planar structures. More electronegative ( $\text{Si} < \text{H} < \text{Ph} < \text{N}$ ) or  $\pi$ -donating substituents induce more trans-bending and longer Al=Al bonds. NHC-coordinated dialumenes always have shorter and more planar Al=Al bonds than their  $\text{PMe}_3$  counterparts (Al=Al = 2.42–2.48 Å vs. 2.45–2.60 Å).

These substituent effects mimic those in disilenes, reflecting the isoelectronic relationship between  $\text{R}_2\text{Si}=\text{SiR}_2$  and  $\text{R(L)Al}=\text{Al(L)R}$ . In disilenes, trans-bend angles and Si=Si bond distances are correlated with the singlet-triplet energy gap ( $\Delta E_{\text{S-T}}$ ) of the notional or real silylene monomers,  $:\text{SiR}_2$ .<sup>[17]</sup> We find that the same relationship applies to dialumenes: Al=Al bond dissociation energy increases as  $\Delta E_{\text{S-T}}$  for the monomeric  $\text{R(L)Al}:$  fragments decreases (Figure S11). The result is that dialumene bond dissociation energy/geometry can be predicted based on properties of the  $\text{R(L)Al}:$  (aluminum) monomer.

We attribute the stronger and more planar Al=Al bonds of NHC- vs.  $\text{PMe}_3$ -coordinated dialumenes to the strong



**Table 1:** Selected geometrical and thermodynamic properties of model dialumenes calculated at SMD-B3LYP-D3/6-311G(2d,2p)//M062X-D3/def2SVP level<sup>[a]</sup>

Al=Al [Å]	2.42	2.44	2.39	2.48	2.45	2.47	2.46	2.60
L-Al-R [°]	101.7	97.1	112.1/106.9	91.9	95.8	92.7	98.7	99.4
$\theta$ [°] <sup>[b]</sup>	29.6/47.2 <sup>[d]</sup>	33.4/53.9 <sup>[e]</sup>	19.1/16.3 <sup>[f]</sup>	43.1	46.6	50.5/50.4	41.6/41.0	63.5/44.6 <sup>[g]</sup>
$\Delta G_{298}(\text{dissoc})$ [kcal mol <sup>-1</sup> ] <sup>[c]</sup>	22.1	20.6	33.2	11.5	19.3	19.7	25.5	2.1
$\Delta E_{S-T}(\text{monomer})$ [kcal mol <sup>-1</sup> ]	19.2	20.6	12.3	25.5	23.2	25.4	16.4	32.4

[a] L = NHC, Imidazol-2-ylidene (C<sub>3</sub>H<sub>4</sub>N<sub>2</sub>). [b]  $\theta$  = trans-bend angle, see Figure 2. Unless otherwise noted,  $\tau = 0^\circ$ . Where two values are listed, complexes are unsymmetrically trans-bent. [c] corrected for basis set superposition error (Table S7). [d]  $\tau = 17.8^\circ$ . [e]  $\tau = 20.5^\circ$ . [f]  $\tau = 7.9^\circ$ . [g]  $\tau = 19.8^\circ$ .

donor ability of the NHC, which raises the R(L)Al: HOMO, narrowing  $\Delta E_{S-T}$ . In contrast, the low dissociation energy for Me<sub>2</sub>N(PMe<sub>3</sub>)Al=Al(PMe<sub>3</sub>)NMe<sub>2</sub>, (2.1 kcal mol<sup>-1</sup>) is explained by the large  $\Delta E_{S-T}$  for the Me<sub>2</sub>N(Me<sub>3</sub>P)Al: fragment (32.4 kcal mol<sup>-1</sup>).

Returning to dialumene **1**, we can ascribe its extreme trans-bending to the electronegative/ $\pi$ -donating NR<sub>2</sub> substituent and narrow 85° N1-Al1-P1 angle enforced by the ligand, which both increase  $\Delta E_{S-T}$  in the monomeric aluminyl fragment (Table S9). Calculations on the full dialumene **1** predict a bond dissociation energy of 7.1 kcal mol<sup>-1</sup>, vs. 25.0 and 19.0 kcal mol<sup>-1</sup> for **I** and **II** (Table S7). To explore the possible dissociation of **1**, we turned to its solution-phase behaviour.

Dialumene **1** is predominantly dimeric in solution. Its <sup>31</sup>P{<sup>1</sup>H} NMR spectrum at 300 K has one broad signal at  $\delta$  21.3 ( $\Delta\nu_{1/2} = 134$  Hz) (Figure 4a). <sup>1</sup>H NMR spectroscopy reveals two ligand environments for **1**, in the ratio 54%:46%, indicating at least two (stereo)isomers. The stereogenic Al centres of **1**, in combination with its ligand backbone, mean that there are three possible diastereomers of *E*-**1**, **A-C** (Figures 4a, S1), each of which must have distinct <sup>31</sup>P signals.<sup>[18]</sup> **1A** and **1B** are *meso* compounds with equivalent phosphorus centres—each will give rise to a singlet. **1C** has inequivalent phosphorus centres, so two <sup>31</sup>P resonances (potentially doublets with <sup>3</sup>J<sub>PP</sub>). The pattern of DFT-predicted <sup>31</sup>P signals confirms our stereochemical analysis (Figure 4c, S15).

At 300 K, the broad <sup>31</sup>P{<sup>1</sup>H} resonance at  $\delta$  21.3 indicates diastereomers **1A-C** are exchanging. Cooling to 243 K, resolves this broad signal into two singlets ( $\delta$  20.4 and  $\delta$  20.0). At 203 K, the higher field signal ( $\delta$  19.5) broadens and approaches coalescence ( $\Delta\nu_{1/2} = 148$  Hz).

The dynamic <sup>31</sup>P{<sup>1</sup>H} NMR behaviour of **1** arises from a combination of intra- and intermolecular exchange processes that exchange diastereomers **1A-C**. In the low temperature regime ( $\lesssim 300$  K), only intramolecular fluxional processes are operative. The two singlets observed at 243 K are assigned to **1A/B** and **1C**. A “trans-flip” process, fast on the NMR timescale at this temperature, simultaneously inverts the stereochemistry at both aluminium centres (Figure 4b). This has the effect of interconverting diastereomers **1A** and **1B**, generating a (concentration-weighted) time-averaged signal for them. In **1C**, the trans-flip is instead a degenerate

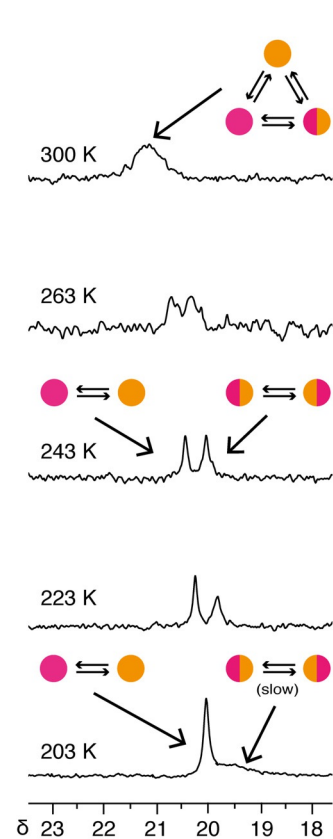
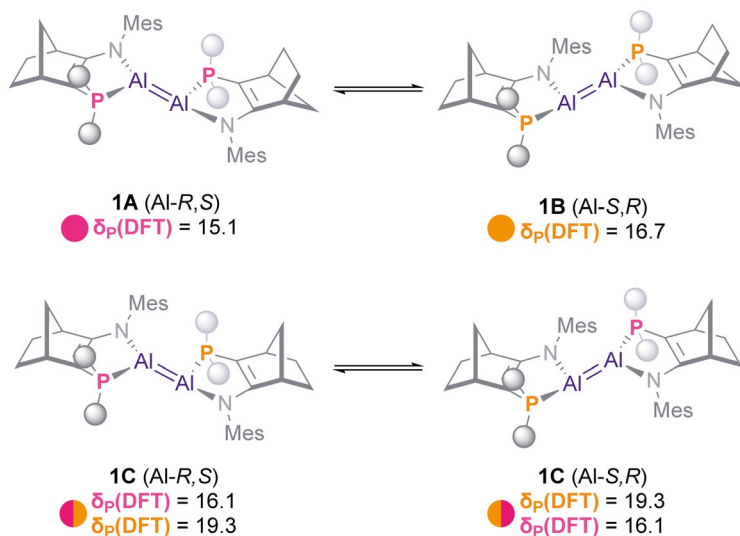
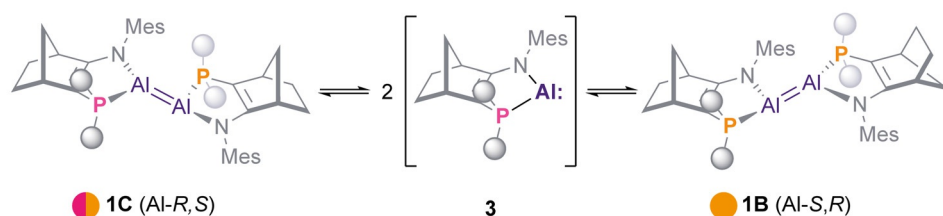
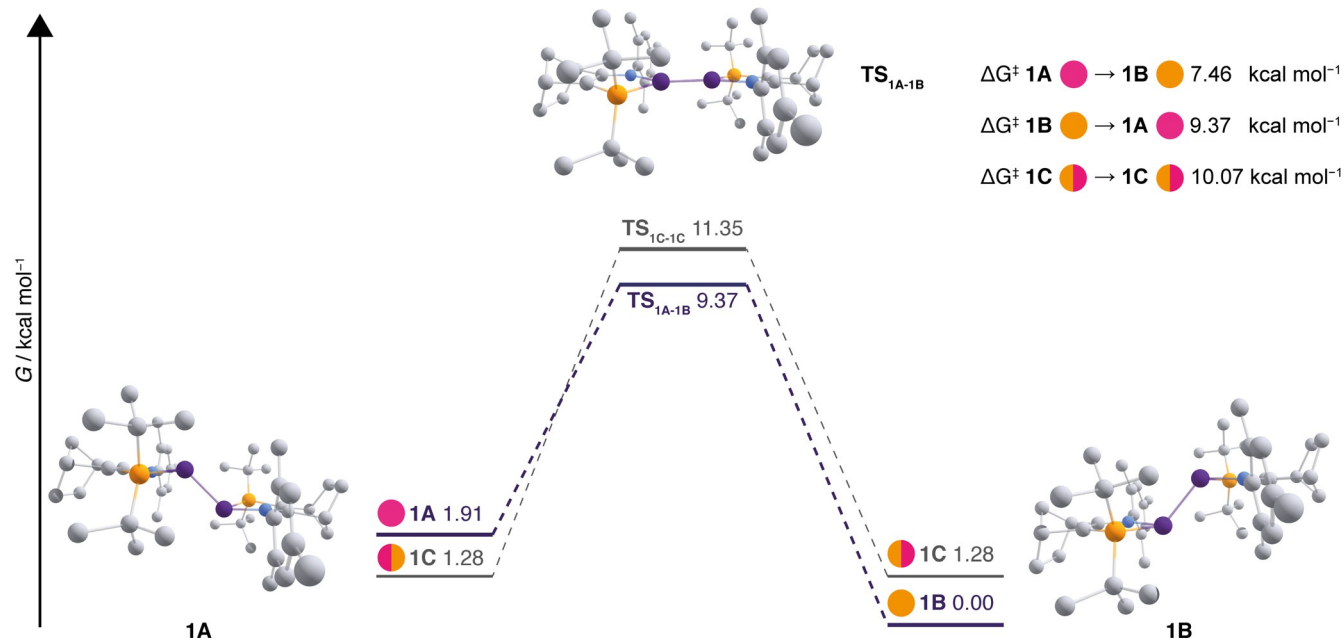
process that exchanges the two inequivalent phosphorus centres, leading to the observed singlet. At 203 K, we assign the broad signal to **1C**, in which the trans-flip is becoming slow on the NMR timescale.

Using DFT calculations we were able to locate the planar transition states **TS<sub>1A-1B</sub>** and **TS<sub>1C-1C</sub>** for the trans-flip process (Figure 4d). The barriers for this process range from 8 to 11 kcal mol<sup>-1</sup>. **TS<sub>1C-1C</sub>** is higher in energy than **TS<sub>1A-1B</sub>** (11.35 vs. 9.37 kcal mol<sup>-1</sup>).

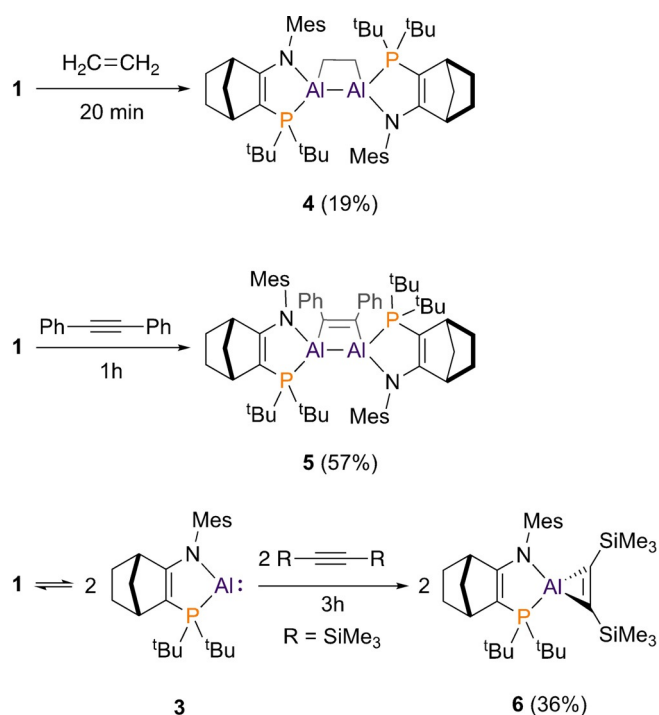
In the higher temperature regime ( $\sim 300$  K), exchange between isomers **1A/B** and **1C** becomes active through an intermolecular route. Dissociation of dialumene **1** generates monomeric aluminyl **3**, which can then recombine to form any of the three diastereomers of **1** (Figure 4c). This process is possible due to the low dissociation energy of **1**, (DFT predicts  $\Delta G_{298} = +7.1$  kcal mol<sup>-1</sup>). 2D <sup>1</sup>H EXSY NMR spectroscopy at 300 K reveals exchange cross peaks between resonances for **1A/1B** (time averaged) and **1C** (Figures S6/7). Our DFT calculations place diastereomers **1A-C** very close in energy, spanning just 2 kcal mol<sup>-1</sup>. Experimental measurements are consistent with this. We were able to determine the equilibrium constants for the exchange of [**1A + 1B**] with **1C** in the temperature range 188–243 K (Figure S5). We can thus estimate  $\Delta G^0$  for [**1A + 1B**]  $\rightarrow$  **1C** as  $0.8 \pm 0.2$  kJ mol<sup>-1</sup> ( $0.19 \pm 0.04$  kcal mol<sup>-1</sup>).

The presence of aluminyl **3** in solution is revealed by dynamic NMR behaviour, but its concentration must be rather low since we did not observe signals for it. Nor did UV-vis spectroscopy in the temperature range 5–65°C reveal absorptions for **3** (Figure S3). Lacking direct spectroscopic evidence, we sought to trap **3**.

Like **I** and **II**,<sup>[3]</sup> **1** can react with alkenes and alkynes to form 4-membered aluminacycles. Treatment of **1** with ethene (1 atm) at room temperature results in rapid (5–20 mins) conversion to dialuminacyclobutane **4** by formal [2+2] cycloaddition of the Al=Al and C=C bonds. Similarly, diphenylacetylene reacts with **1** to form dialuminacyclobutene **5** (Scheme 2). <sup>31</sup>P{<sup>1</sup>H} NMR spectroscopy of **4** and **5** reveals distinct signals for three diastereomers in each case. This is a result of the “locking” of the stereogenic aluminium centres enforced by their cyclic structures (**4**:  $\delta$  11.6 (d, <sup>3</sup>J<sub>PP</sub> = 12 Hz), 11.5 (s), 11.5 (s), 11.4 (d, <sup>3</sup>J<sub>PP</sub> = 12 Hz); **5**:  $\delta$  11.0 (br s), 10.7 (s), 10.4 (s), 10.3 (br s).; see SI).

a) VT  $^{31}\text{P}\{^1\text{H}\}$  spectroscopy of **1**b) Inversion at Al exchanges diastereomers **1A** and **1B**c) Dissociation and recombination exchanges diastereomers **1A/B** and **1C**d) Reaction profile for 'trans-flip' isomerisation in **1**

**Figure 4.** a)  $^{31}\text{P}\{^1\text{H}\}$  NMR spectra of **1** (161 MHz,  $[\text{D}_8]\text{toluene}$ ) recorded at 203–300 K. b) Inversion at aluminium exchanges **1A** and **1B**, but is degenerate for **1C**. c) Intermolecular dissociation/recombination of **1** exchanges all diastereomers. d) Reaction energy profile for the “trans-flip” in diastereomers **1A-C** at  $T=298.15$  K (geometries optimised at M062X-D3/def2SVP, energies calculated at B3LYP-D3/6-311G(2d,2p) corrected for  $\text{C}_6\text{H}_6$  solvent).



**Scheme 2.** Reactivity of dialumene **1** with alkenes/alkynes.

X-ray crystallography reveals the geometry of the  $\text{C}_2\text{Al}_2$  rings of **4** and **5**. The Al–Al distances in **4** and **5** are not notably longer than in **1**, despite destruction of the Al=Al  $\pi$  bond (**1**, 2.519(1) Å; **4**, 2.558(1) Å; **5**, 2.512(1) Å, see SI). This is rather different to the behaviour of dialumenes **I** or **II** in comparable reactions with alkenes/alkynes. The resulting analogues of **4/5** exhibit substantial Al–Al bond elongation (0.20–0.25 Å) compared to **I/II**. The difference reflects the lower Al=Al bond order in **1** vs. **I/II**.

When dialumene **1** is treated with the bulkier alkyne  $\text{Me}_3\text{SiC}\equiv\text{CSiMe}_3$ , the observed product is derived not from **1** but rather from its monomer, **3**. On addition of  $\text{Me}_3\text{SiC}\equiv\text{CSiMe}_3$ , purple solutions of **1** become yellow within three hours.  $^{31}\text{P}\{^1\text{H}\}$  NMR reveals a broad signal at  $\delta$  9.8, characteristic of amidophosphine-coordinated Al(III) compounds.<sup>[19]</sup>

X-ray crystallography shows that the product from **1** and  $\text{Me}_3\text{SiC}\equiv\text{CSiMe}_3$  is aluminacyclopropene **6** (Figure 5). **6** has the narrow C1–Al–C2 angle expected for aluminacyclopropenes ( $42.05(9)^\circ$ ) and its C1=C2 distance is typical for a double bond (1.367(2) Å). Cycloaddition reactions with alkynes are a characteristic reaction for neutral aluminyls. A NacNac-coordinated analogue of **6** has been prepared by reduction of Al(III) precursors in the presence of  $\text{Me}_3\text{SiC}\equiv\text{CSiMe}_3$ , though with other alkynes direct reaction with NacNacAl(I) is also viable.<sup>[20]</sup> Structurally, the  $\text{AlC}_2$  core of **5** and its NacNac analogue are closely comparable.

## Conclusion

In summary, we have prepared the first isolable dialumene that dissociates in solution. The donor properties of the amidophosphine ligand generate a large  $\Delta E_{\text{S-T}}$  on the

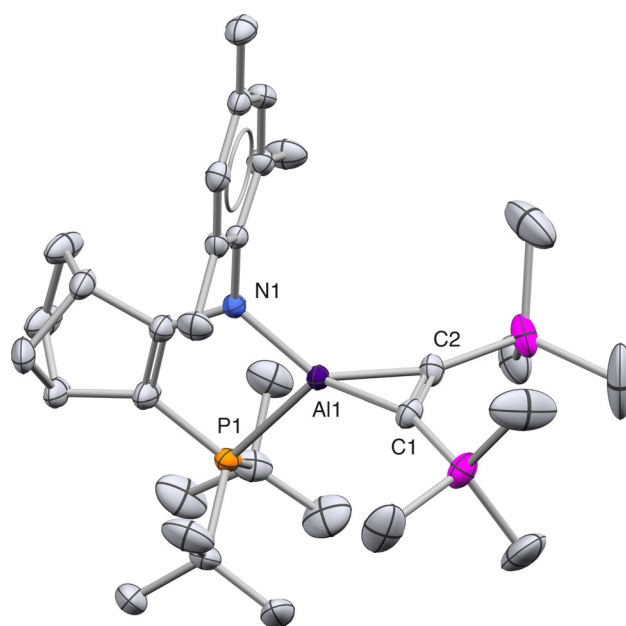


**Figure 5.** X-ray crystal structure of aluminacyclopropene **6** (H atoms omitted). Thermal ellipsoids at 50% probability. The asymmetric unit comprises two molecules; just one is shown.

transient aluminyl monomers. This large  $\Delta E_{\text{S-T}}$  is the origin of the low bond order, high trans-bending, and weak Al=Al bond in **1**. We continue to explore the reactivity of **1** and related systems.

## Acknowledgements

This project received funding from the European Research Council (ERC) under the EU Horizon 2020 research and innovation programme (ERC-2016-STG-716315). We acknowledge the Irish Centre for High-End Computing for computational facilities and support. K.M.B. thanks MU for a Graduate Teaching Scholarship.

## Conflict of Interest

The authors declare no conflict of interest.

**Keywords:** aluminium · aluminium(I) compounds · dialumene · low-valent atoms · multiple bonds

[1] a) P. P. Power, *Nature* **2010**, *463*, 171–177; b) C. Weetman, *Chem. Eur. J.* **2021**, *27*, 1941–1954.

[2] a) C. Dohmeier, C. Robl, M. Tacke, H. Schnöckel, *Angew. Chem. Int. Ed. Engl.* **1991**, *30*, 564–565; *Angew. Chem.* **1991**, *103*, 594–595; b) C. Cui, H. W. Roesky, H. G. Schmidt, M. Noltemeyer, H. Hao, F. Cimpoesu, *Angew. Chem. Int. Ed.* **2000**, *39*, 4274–4276; *Angew. Chem.* **2000**, *112*, 4444–4446; c) J. Hicks, P. Vasko, J. M. Goicoechea, S. Aldridge, *Angew. Chem. Int. Ed.* **2021**, *60*, 1702–1713; *Angew. Chem.* **2021**, *133*, 1726–1737.

- [3] a) P. Bag, A. Porzelt, P. J. Altmann, S. Inoue, *J. Am. Chem. Soc.* **2017**, *139*, 14384–14387; b) C. Weetman, A. Porzelt, P. Bag, F. Hanusch, S. Inoue, *Chem. Sci.* **2020**, *11*, 4817–4827.
- [4] a) R. J. Wright, A. D. Phillips, P. P. Power, *J. Am. Chem. Soc.* **2003**, *125*, 10784–10785; b) the same dialumene may also be trapped by alkynes. C. Cui, X. Li, C. Wang, J. Zhang, J. Cheng, X. Zhu, *Angew. Chem. Int. Ed.* **2006**, *45*, 2245–2247; *Angew. Chem.* **2006**, *118*, 2303–2305.
- [5] T. Agou, K. Nagata, N. Tokitoh, *Angew. Chem. Int. Ed.* **2013**, *52*, 10818–10821; *Angew. Chem.* **2013**, *125*, 11018–11021.
- [6] a) K. Nagata, T. Agou, N. Tokitoh, *Angew. Chem. Int. Ed.* **2014**, *53*, 3881–3884; *Angew. Chem.* **2014**, *126*, 3962–3965; b) T. Agou, K. Nagata, T. Sasamori, N. Tokitoh, *Phosphorus Sulfur Silicon Relat. Elem.* **2016**, *191*, 588–590; c) K. Nagata, T. Murosaki, T. Agou, T. Sasamori, T. Matsuo, N. Tokitoh, *Angew. Chem. Int. Ed.* **2016**, *55*, 12877–12880; *Angew. Chem.* **2016**, *128*, 13069–13072.
- [7] C. Weetman, P. Bag, T. Szilvási, C. Jandl, S. Inoue, *Angew. Chem. Int. Ed.* **2019**, *58*, 10961–10965; *Angew. Chem.* **2019**, *131*, 11077–11081.
- [8] a) J. Moilanen, P. P. Power, H. M. Tuononen, *Inorg. Chem.* **2010**, *49*, 10992–11000; b) for a review of related systems see E. Rivard, P. P. Power, *Inorg. Chem.* **2007**, *46*, 10047–10064.
- [9] T. Agou, K. Nagata, T. Sasamori, N. Tokitoh, *Chem. Asian J.* **2014**, *9*, 3099–3101.
- [10] J. D. Queen, A. Lehmann, J. C. Fettinger, H. M. Tuononen, P. P. Power, *J. Am. Chem. Soc.* **2020**, *142*, 20554–20559.
- [11] R. L. Falconer, G. S. Nichol, I. V. Smolyar, S. L. Cockroft, M. J. Cowley, *Angew. Chem. Int. Ed.* **2021**, *60*, 2047–2052; *Angew. Chem.* **2021**, *133*, 2075–2080.
- [12] W. Uhl, *Z. Naturforsch.* **1988**, *43b*, 1113–1118.
- [13] H. Grützmacher, T. F. Fässler, *Chem. Eur. J.* **2000**, *6*, 2317–2325.
- [14] By calculating  $\delta(\text{Al}, \text{Al})_{\text{I}}/\delta(\text{Al}, \text{Al})_{\text{VI}}$  we can estimate the Al–Al bond order in **1** as 1.24. For details see: D. B. Chesnut, *Chem. Phys.* **2006**, *321*, 269–276.
- [15] C. Gatti, *Z. Kristallogr.* **2005**, *220*, 399–457.
- [16] For calculations on  $(\text{NHC})_2\text{Al}_2\text{X}_2$  systems see N. Holzmann, A. Stasch, C. Jones, G. Frenking, *Chem. Eur. J.* **2011**, *17*, 13517–13525.
- [17] For a summary see a) M. Kira, T. Iwamoto, *Adv. Organomet. Chem.* **2006**, *54*, 73–148. Initial reports: b) E. A. Carter, W. A. Goddard, *J. Phys. Chem.* **1986**, *90*, 998–1001; c) J. P. Malrieu, G. Trinquier, *J. Am. Chem. Soc.* **1989**, *111*, 5916–5921; d) M. Karni, Y. Apeloig, *J. Am. Chem. Soc.* **1990**, *112*, 8589–8590.
- [18] Z isomers of **1** are ruled out on the basis of their higher energy, see SI.
- [19] R. L. Falconer, G. S. Nichol, M. J. Cowley, *Inorg. Chem.* **2019**, *58*, 11439–11448.
- [20] a) H. Zhu, R. B. Oswald, H. Fan, H. W. Roesky, Q. Ma, Z. Yang, H. Schmidt, M. Noltemeyer, K. Starke, N. S. Hosmane, *J. Am. Chem. Soc.* **2006**, *128*, 5100–5108; b) C. Cui, S. Koepke, R. Herbst-Irmer, H. W. Roesky, M. Noltemeyer, H.-G. Schmidt, B. Wrackmeyer, *J. Am. Chem. Soc.* **2001**, *123*, 9091–9098; c) **6** is also related to the 2- $\pi$  aromatic aluminacyclopropenes discussed in a recent review, see: K. Ota, R. Kinjo, *Chem. Rev.* **2021**, *121*, 10594–10673.
- [21] Deposition Numbers 2100531 (for **1**), 2100549 (for **4**), 2100550 (for **5**), and 2100551 (for **6**) contain the supplementary crystallographic data for this paper. These data are provided free of charge by the joint Cambridge Crystallographic Data Centre and Fachinformationszentrum Karlsruhe Access Structures service [www.ccdc.cam.ac.uk/structures](http://www.ccdc.cam.ac.uk/structures).

Manuscript received: August 23, 2021

Accepted manuscript online: September 14, 2021

Version of record online: October 7, 2021